Dynamical instabilities and transient short-range order in the fermionic Hubbard model

Johannes Bauer,[1] Mehrtash Babadi,[2] and Eugene Demler[1]
[1]*Department of Physics, Harvard University, Cambridge, Massachusetts 02138, USA*
[2]*Institute for Quantum Information and Matter, Caltech, Pasadena, CA 91125*
(Received 10 December 2014; published 27 July 2015)

We study the dynamics of magnetic correlations in the half-filled fermionic Hubbard model following a fast ramp of the repulsive interaction. We use Schwinger-Keldysh self-consistent second-order perturbation theory to investigate the evolution of single-particle Green's functions and solve the nonequilibrium Bethe-Salpeter equation to study the dynamics of magnetic correlations. This approach gives us new insights into the interplay between single-particle relaxation dynamics and the growth of antiferromagnetic correlations. Depending on the ramping time and the final value of the interaction, we find different dynamical behavior which we illustrate using a dynamical phase diagram. Of particular interest is the emergence of a transient short-range ordered regime characterized by the strong initial growth of antiferromagnetic correlations followed by a decay of correlations upon thermalization. The discussed phenomena can be probed in experiments with ultracold atoms in optical lattices.

DOI: 10.1103/PhysRevB.92.024305 PACS number(s): 71.30.+h, 71.27.+a, 71.10.Fd, 71.10.Hf

I. INTRODUCTION

Nonequilibrium dynamics of quantum many-body systems has been the subject of experimental inquiry in many areas of physics in recent years. For example, pump-probe experiments in solid-state systems have addressed such important issues as the observation of the Higgs mode in superconductors [1,2] and the identification of dominant couplings in cuprate superconductors [3–6]. A particularly exciting direction is the dynamical generation, suppression, or manipulation of ordered phases using external fields. Nonequilibrium induced superconductivity [7,8] in cuprate compounds, ultrafast melting of charge-density-wave order [9–11], transient generation of spin-density-wave order in pnictides [12], and ultrafast manipulation of the order in multiferroics [13] are examples of such possibilities.

Artificial systems of ultracold atoms allow a clean and tunable experimental realization of the paradigmatic condensed matter models that underlie many solid-state systems. In these experiments, microscopic parameters can be rapidly changed using external fields and nonequilibrium quantum dynamics can be probed [14–24]. For example, in Ref. [18] Jo *et al.* reported an experimental study of the possible occurrence of the Stoner ferromagnetic instability following a rapid interaction quench to the BEC side of a Feshbach resonance with large positive scattering length (for subsequent experiments and analysis see Refs. [21,25]).

Here we study dynamical instabilities and the growth of magnetic correlations in the repulsive fermionic Hubbard model following an interaction ramp. At half-filling, the paramagnetic (PM) state is unstable toward antiferromagnetic (AFM) ordering for weak on-site repulsion at low temperatures [see Figs. 1(a) and 1(b)]. This permits a controlled perturbative analysis. One of the central findings of our study is the identification of an extended parameter regime in which the prethermal state that emerges after the interaction ramp [26,27] exhibits growing AFM correlations, and can develop sizable domains with short-range AFM order; interestingly, these features are only transient and decay when the thermal equilibrium state is approached [see Figs. 1(d) and 1(e)]. Phenomenologically, "transient short-range order" (TSO) in the present context can be understood by first noting that at half-filling, the logarithmic divergence of the spin susceptibility that results from Fermi surface nesting is only suppressed by finite temperature. The prethermal single-particle momentum distribution $n_{\boldsymbol{k}}^{\mathrm{pt}}$ is found to closely resemble the initial low-temperature distribution $n_{\boldsymbol{k}}^{0}$ for $k \approx k_{\mathrm{F}}$ [27], and thus elicits a strong AFM response and even an instability for large enough on-site repulsion. The instability is maintained for a time inversely proportional to the thermalization rate of the low-energy prethermal quasiparticles. The disordered PM state is eventually recovered as $n_{\boldsymbol{k}}(t)$ slowly approaches the final thermal state in which the generated temperature T_{f} exceeds T_c^{eq}, the critical AFM transition temperature.

Considerable progress has been made in the accurate description of many-body quantum dynamics in one dimension [28–34] and in infinite dimensions using the nonequilibrium extension of dynamical mean field theory (DMFT) [35,36]. The situation is more challenging in two and three dimensions where accurate and efficient methods are not available. Previous works on the nonequilibrium dynamics of the Hubbard model [27,37–40] and itinerant fermions [41] have studied thermalization following interaction ramps, which is found to be preceded by the rapid establishment of a prethermal plateau with a substantially modified $n_{\boldsymbol{k}}$. On another front, the dynamics of the order parameter in quenches has been studied within the integrable BCS theory [42–44]. These works, however, do not take into account single-particle excitations and order parameter fluctuations at finite momentum, both of which break integrability and substantially modify the physics in low dimensions. More recently, quenches from the ordered AFM phase into the normal phase have been analyzed within DMFT [45–47], as well as slow ramps into the AFM state starting with a small seeding field [48]. In the latter case the dynamics of the magnetization was studied, however, the interplay between single-particle properties and the two-particle spin-spin correlation function during the relaxation dynamics was not addressed. We show that this interplay introduces additional complexity and richness to the nonequilibrium dynamics.

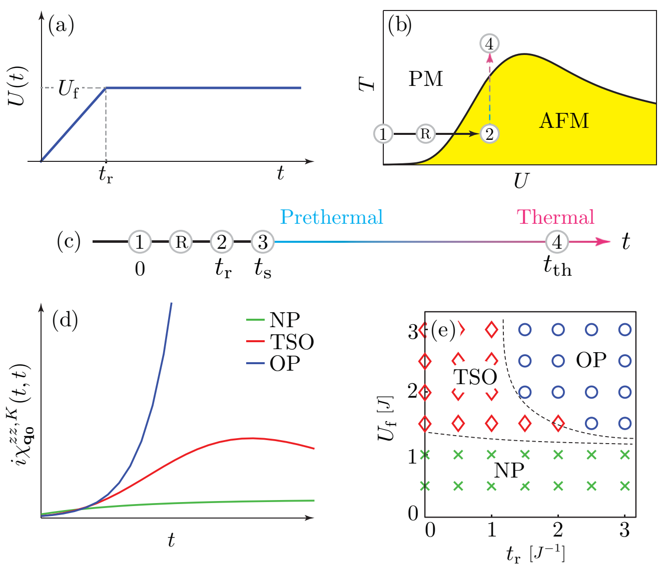

FIG. 1. (Color online) (a) Linear interaction ramp $U(t)$ with ramping time t_r and final interaction U_f. (b) Schematic equilibrium phase diagram showing the paramagnetic phase (PM), the critical temperature $T_c^{\mathrm{eq}}(U)$ for the antiferromagnetic (AFM) phase, and the relaxation trajectory to a final temperature T_f. (c) Time scales and different regimes (see text). (d) Qualitatively different regimes for the evolution of the equal-time AFM correlations; NP: slow growth to normal phase result. TSO: transient short-range order; AFM correlations initially develop and later decay upon thermalization, $T_\mathrm{f} > T_c^{\mathrm{eq}}(U_\mathrm{f})$. OP: AFM correlations grow and final thermalized state expected to be the ordered phase, $T_\mathrm{f} < T_c^{\mathrm{eq}}(U_\mathrm{f})$. (e) The dynamical phase diagram showing different regimes after a ramp from an initial PM state at temperature $T_i = 0$ as a function of U_f and t_r. The dashed lines are meant as a guide to the eye.

II. MODEL AND FORMALISM

We consider the quasi-two-dimensional Hubbard model [49] with nearest neighbor hopping and a time-dependent on-site interaction,

$$H = \sum_{\boldsymbol{k},\sigma} \varepsilon_{\boldsymbol{k}}\, c^\dagger_{\boldsymbol{k},\sigma} c_{\boldsymbol{k},\sigma} + U(t) \sum_i n_{i,\uparrow} n_{i,\downarrow}. \tag{1}$$

The dispersion is $\varepsilon_{\boldsymbol{k}} = -2J(\cos k_x + \cos k_y)$, where J is the nearest neighbor hopping amplitude. We work in the units where $\hbar = k_\mathrm{B} = J = 1$ and assume half-filling $\langle n_\uparrow \rangle = \langle n_\downarrow \rangle = 1/2$ hereafter. The dispersion satisfies the perfect nesting condition $\varepsilon_{\boldsymbol{k}+\boldsymbol{q}_0} = -\varepsilon_{\boldsymbol{k}}$ for $\boldsymbol{q}_0 = (\pi,\pi)$, and the PM state exhibits an AFM instability signaled by the divergence of the static magnetic susceptibility $\chi^{zz}_{\boldsymbol{q}_0}(i\omega = 0)$. At weak coupling, the critical temperature T_c can be estimated within RPA, $T_c \sim J e^{-\sqrt{cJ/U}}$, where c is a numerical constant [50]. Higher order correction analogous to the ones discussed by Gor'kov [51] in the theory of superconductivity are found to be important already at weak coupling and result in an $O(1)$ correction to the prefactor of T_c; this correction can be conveniently captured by replacing $U \to U_\mathrm{eff}$ in the RPA calculation [50,52–55]. A first estimate of the growth rate of the staggered magnetization in the PM state $\Delta_{\boldsymbol{q}_0}$ can be obtained from linear response $\Delta_{\boldsymbol{q}_0} \sim J e^{-\sqrt{\bar{c}J/U_\mathrm{eff}}}$ [25]. Nonlinear corrections quickly become relevant due to the fast single-particle relaxation dynamics, making this result questionable for longer times.

Going beyond linear response, we describe the dynamics within the framework of Φ-derivable approximations [56] and nonequilibrium Green's functions on the Schwinger-Keldysh contour [57–59]. The closed-time-path single-particle Green's function is defined as $\mathcal{G}_{i,\sigma;j,\sigma'}(t,t') = -i\langle T_\mathcal{C}[c_{i,\sigma}(t_1)\, c^\dagger_{j,\sigma'}(t_2)]\rangle$, where $\mathcal{C}$ is the round-trip Schwinger-Keldysh time contour, $t_1,t_2 \in \mathcal{C}$ are contour times, and $T_\mathcal{C}$ is the contour time-ordering operator. The initial state of the system at $t = 0$ is assumed to be a uniform and uncorrelated paramagnet. In this setup the SU(2) and translation symmetry is preserved at all times such that $\mathcal{G}_{i,\sigma;j,\sigma'} \equiv \delta_{\sigma\sigma'} G_{i-j}(t,t')$. Dynamical symmetry breaking requires a weak inhomogeneity or small seeding field, which we do not assume here; rather we probe the growth of magnetic correlations by studying the nonequilibrium spin-spin correlation function $\chi^\mathrm{K}_{\boldsymbol{q}}$, and the growth (instability) of domains from the retarded response $\chi^\mathrm{R}_{\boldsymbol{q}}$.

In the momentum basis, $G_{\boldsymbol{q}}(t,t')$ is obtained by solving the nonequilibrium Dyson equation $G^{-1}_{\boldsymbol{q}}(t,t') = G^{-1}_{0,\boldsymbol{q}}(t,t') - \Sigma_{\boldsymbol{q}}(t,t')$. Here $G^{-1}_{0,\boldsymbol{q}}(t,t') = (i\partial_t - \xi_{\boldsymbol{q}})\,\delta_\mathcal{C}(t,t')$, where $\delta_\mathcal{C}$ is the contour δ function, and the self-energy is obtained as $\Sigma_{\boldsymbol{q}}(t,t') = -\delta\Phi[\mathcal{G}]/\delta G_{-\boldsymbol{q}}(t',t)$, where $\Phi[\mathcal{G}]$ is the Luttinger-Ward functional. We consider ramps to weak final interactions $U_\mathrm{f} < 4J$ such that a skeleton expansion of $\Phi[\mathcal{G}]$ up to the second order in U is justified [48,60]:

$\Phi[\mathcal{G}] =$ 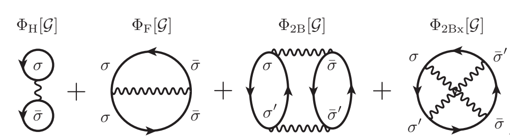 (2)

These vacuum diagrams determine Σ and the irreducible vertex $I(11';22') = \delta^2\Phi[\mathcal{G}]/\delta\mathcal{G}(1'1)\delta\mathcal{G}(22')$ in the particle-hole channel. The latter is used to calculate the spin-spin correlation function $\chi^{\mu\nu}_{\boldsymbol{q}}(t,t') \equiv -i\langle T_\mathcal{C}[\hat{S}^\mu_{\boldsymbol{q}}(t)\, \hat{S}^\nu_{-\boldsymbol{q}}(t')\rangle$ by solving a nonequilibrium Bethe-Salpeter equation. Here $\hat{S}^\mu(\boldsymbol{q}) = \frac{1}{2}\sum_{\boldsymbol{k}} c^\dagger_{\boldsymbol{k}+\boldsymbol{q},\alpha}\, \sigma^\mu_{\alpha\beta}\, c_{\boldsymbol{k},\beta}$, with $\{\sigma^\mu\}$ being the Pauli matrices. The SU(2) symmetry implies $\chi^{\mu\nu}_{\boldsymbol{q}}(t,t') = \frac{1}{2}\,\delta^{\mu\nu}\chi^{+-}_{\boldsymbol{q}}(t,t')$, where χ^{+-} is the transverse spin-spin correlator and its diagrammatic calculation is more economical than the diagonal correlators.

Carrying out such calculations in real time and on a dense two-dimensional momentum grid is numerically extremely challenging, even for low order Φ-derivable approximations. We therefore make additional simplifying approximations to proceed. First, we approximate the irreducible vertices by their local parts, i.e., $\Sigma_{\boldsymbol{q}}(t,t') \to \Sigma_\ell(t,t')$, where $\Sigma_\ell(t,t')$ is a $\boldsymbol{q}$-independent self-energy similar as in DMFT. The local approximation captures the full temporal structure of the vertices while significantly simplifying the forthcoming analysis. Also, the momentum dependence of $\Sigma_{\boldsymbol{q}}$ is known to be fairly weak at weak coupling [55,61,62]. The SU(2) symmetry of the state implies $\Sigma_\mathrm{F} = \Sigma_\mathrm{2Bx} = 0$, and we find

$\Sigma_\ell(t,t') =$ 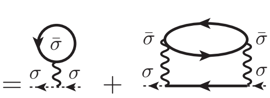 $= U(t)\, n\, \delta_\mathcal{C}(t,t')$

$$- U(t)\, U(t')\, G_\ell(t,t')\, \Pi^\mathrm{ph}_\ell(t,t'), \tag{3}$$

where $n = 1/2$ is the filling, $G_\ell(t,t') = \frac{1}{N}\sum_{\boldsymbol{q}} G_{\boldsymbol{q}}(t,t')$ is the local Green's function, and $\Pi^{\rm ph}_\ell(t,t') = G_\ell(t,t')\,G_\ell(t',t)$. The Hartree term only gives a dynamical phase and can be gauged out using the particle-hole symmetry of the half-filled state. The second-order self-energy, however, is nontrivial and describes the single-particle relaxation dynamics. The transverse spin correlator in the framework of Φ-derivable approximations is obtained by supplementing the real-time action with a fictitious transverse magnetic field term $-\int_{\mathcal{C}} dt \sum_{\boldsymbol{q}} B_{\boldsymbol{q}}(t)\,\hat{S}^-_{-\boldsymbol{q}}(t)$ and calculating the induced linear variation in the Green's function $\chi^{+-}_{\boldsymbol{q}}(t_1,t_2;t') \equiv \delta\,\mathrm{Tr}[\mathcal{G}_{\boldsymbol{q}}(t_1,t_2;B)\,S^+]/\delta B_{\boldsymbol{q}}(t')$. The result is a contour Bethe-Salpeter equation (BSE),

$$\chi^{+-}_{\boldsymbol{q}}(t_1,t_2;t') = \Pi^{\rm ph}_{\boldsymbol{q}}(t_1,t_2;t'^{+},t') + \int_{\mathcal{C}} dt_1' \times \int_{\mathcal{C}} dt_2'\,\Pi^{\rm ph}_{\boldsymbol{q}}(t_1,t_2;t_1',t_2')\,I_\ell(t_1',t_2')\,\chi^{+-}_{\boldsymbol{q}}(t_2',t_1';t'), \quad (4)$$

where $\Pi^{\rm ph}_{\boldsymbol{q}}(t_1,t_2;t_1',t_2') = \frac{1}{N}\sum_{\boldsymbol{k}} G_{\boldsymbol{k}+\boldsymbol{q}}(t_1,t_1')\,G_{\boldsymbol{k}}(t_2',t_2)$ and $I_\ell(t_1,t_2) = I_{\rm F}(t_1,t_2) + I_{\rm 2Bx}(t_1,t_2)$:

$I_\ell(t_1,t_2) =$ 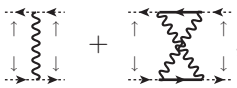 , (5)

is the local irreducible vertex, consisting of a Fock (ladder) part $I_{\rm F}(t_1,t_2) = iU(t_1)\,\delta_{\mathcal{C}}(t_1,t_2)$, and a second-order Gor'kov part $I_{\rm 2Bx}(t_1,t_2) = -U(t_1)\,U(t_2)\,\Pi^{\rm pp}_\ell(t_1,t_2)$, where $\Pi^{\rm pp}_\ell(t_1,t_2) = G_\ell(t_1,t_2)\,G_\ell(t_1,t_2)$. These vertex parts arise from $\Phi_{\rm F}$ and $\Phi_{\rm 2Bx}$ vacuum diagrams, respectively. Finally, the transverse spin correlator is calculated as $\chi^{+-}_{\boldsymbol{q}}(t,t') \equiv \chi^{+-}_{\boldsymbol{q}}(t,t^+;t')$.

Even in the local approximation, the numerical solution of Eq. (4) for the three-time function $\chi^{+-}_{\boldsymbol{q}}(t_1,t_2;t')$ is formidable and requires the inversion of very large matrices. Had the vertex $I_{\rm 2Bx}(t_1',t_2')$ been local in time (as in $I_{\rm F}$), the BSE in Eq. (4) could be immediately reduced to a numerically tractable integral equation for the two-time correlator $\chi^{+-}_{\boldsymbol{q}}(t,t')$, with only one intermediate contour integral. This motivates us to approximately incorporate the role of $I_{\rm 2Bx}$ vertex correction via an effective time-local vertex. For temperatures $T \ll W$ (bandwidth $= 8J$) and near-equilibrium states, the spread of $I_{\rm 2Bx}(t,t')$ on $t - t'$ is of the order of W^{-1}, which is considerably smaller than $\Delta^{-1}_{\boldsymbol{q}_0}$, the inverse growth rate mentioned before. Therefore, beyond the numerical reduction of the nonequilibrium instability rate, no qualitatively distinct behavior is expected to emerge as a matter of the temporal nonlocality of the vertex $I_{\rm 2Bx}$. As mentioned before, the equilibrium Gor'kov correction can be obtained by replacing $U \to U_{\rm eff}[U]$ in the RPA calculation [50,52–54], where $U_{\rm eff}[U]$ is found by requiring that the correct AFM transition temperature is reproduced. Here we assume that the same approximate picture holds for the weak-coupling nonequilibrium dynamics as well, and use the equilibrium effective interaction as a time-local vertex, albeit at the instantaneous value of $U(t)$, i.e., $I_\ell(t_1,t_2) \to iU_{\rm eff}[U(t_1)]\,\delta_{\mathcal{C}}(t_1,t_2)$. This allows us to set $t_2 = t_1^+$ in Eq. (4) and simplify it to

$$\chi^{+-}_{\boldsymbol{q}}(t,t') = \Pi^{\rm ph}_{\boldsymbol{q}}(t,t') + \int_{\mathcal{C}} dt''\,\Pi^{\rm ph}_{\boldsymbol{q}}(t,t'')\,iU_{\rm eff}[U(t'')]\,\chi^{+-}_{\boldsymbol{q}}(t'',t'), \quad (6)$$

where $\Pi^{\rm ph}_{\boldsymbol{q}}(t,t') = \Pi^{\rm ph}_{\boldsymbol{q}}(t,t^+;t'^+,t')$. For the numerical solution of the nonequilibrium Dyson equation and the above BSE, see [55].

III. RESULTS AND DISCUSSION

For concreteness we consider an uncorrelated PM state at initial temperature $T_{\rm i} = 0$ subject to a linear interaction ramp to a final value of $U_{\rm f}$ within a time interval $t_{\rm r}$ [Fig. 1(a)]. The timeline of the single-particle dynamics is shown schematically in Fig. 1(c). Following the ramp, a brief switching regime with a duration $t_s \sim 1/J$ is observed [38] which leads to a prethermal single-particle momentum distribution $n^{\rm pt}_{\boldsymbol{k}}$ that deviates from the initial distribution by $O(U_{\rm f}^2)$ [27]. Collisions slowly smear $n^{\rm pt}_{\boldsymbol{k}}$ to a thermal distribution (see Fig. 2). The thermalization rate of the low-energy quasiparticles is found as $\gamma_{\rm th} \sim U_{\rm f}^4/J^3$ for short ramps, and a smaller value $\gamma_{\rm th} \sim U_{\rm f}^4/(J^5 t_{\rm r}^2)$ for long ramps [38]. The final temperature $T_{\rm f}$ generically increases with $U_{\rm f}$ and decreases with $t_{\rm r}$. We monitor the evolution of the single-particle momentum distribution $n_{\boldsymbol{k}}(t)$, and the equal-time Keldysh correlator $\chi^{\rm K}_{\boldsymbol{q}}(t,t) = -i\langle\{\hat{S}^+_{\boldsymbol{q}}(t),\hat{S}^-_{-\boldsymbol{q}}(t)\}\rangle$, and the retarded spin correlator $\chi^{\rm R}_{\boldsymbol{q}}(t,t') = -i\theta(t-t')\langle[\hat{S}^+_{\boldsymbol{q}}(t),\hat{S}^-_{-\boldsymbol{q}}(t')]\rangle$.

We identify qualitatively different behaviors depending on $U_{\rm f}$ and $t_{\rm r}$, which is concisely collected in the dynamical phase diagram shown in Fig. 1(e). The symbols (NP, $\times$) correspond

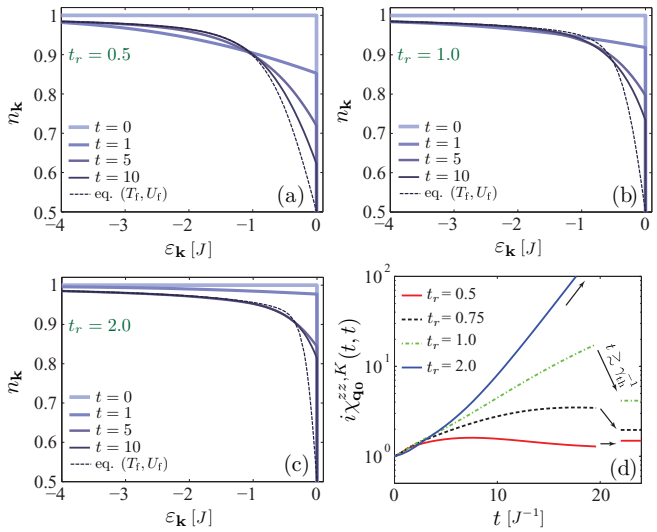

FIG. 2. (Color online) Momentum distribution function $n_{\boldsymbol{k}}(t)$ for $T_{\rm i} = 0$, $U_{\rm f} = 3$ and different ramping times. (a) $t_{\rm r} = 0.5$, $T_{\rm f} \approx 0.29 > T_c^{\rm eq}$, (b) $t_{\rm r} = 1.5$, $T_{\rm f} \approx 0.15 > T_c^{\rm eq}$, and (c) $t_{\rm r} = 2$, $T_{\rm f} \approx 0.08 < T_c^{\rm eq}$. The dotted lines show the final equilibrium $n_{\boldsymbol{k}}$ at $T = T_{\rm f}$. (d) The time dependence of $\chi^{zz,{\rm K}}_{\boldsymbol{q}_0}(t,t)$ for different $t_{\rm r}$ in TSO and OP regime (semilog plot). The long-time limit of the correlators in the TSO regime is shown on the plot from an equilibrium calculation at $T = T_{\rm f}$ [63].

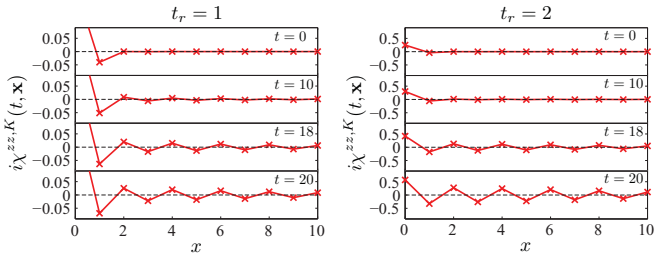

FIG. 3. (Color online) Equal time spatial spin correlation function $i\chi^{\mathrm{K}}(t,x)$ for $t_{\mathrm{r}} = 1$ (left, TSO), and $t_{\mathrm{r}} = 2$ (right, OP) for $T_{\mathrm{i}} = 0$ and $U_{\mathrm{f}} = 3$ for different times t and lattice spacing $a = 1$. Notice the different scale on the vertical axis.

to weak growth, (TSO, $\diamond$) to transient AFM correlations along with a PM state upon thermalization, and (OP, $\circ$) to AFM ordered phase upon thermalization.

The evolution of the AFM correlations for each of these dynamical modalities is shown schematically in Fig. 1(d). The NP regime is identified by a monotonic growth of the equal-time spin correlator $\chi^{\mathrm{K}}_{\boldsymbol{q}}$ to its final equilibrium value and being bounded by it, along with a decaying spin response ($\chi^{\mathrm{R}}_{\boldsymbol{q}}$, see [55]) for all modes. In the TSO regime, one observes an enhancement of AFM correlations for intermediate times $t_{\mathrm{s}} \lesssim t \lesssim \gamma_{\mathrm{th}}^{-1}$; in this regime, AFM seeds can rapidly grow into sizable domains as signaled by the exponentially growing retarded response function. These features eventually subside at longer times $t \gtrsim \gamma_{\mathrm{th}}^{-1}$ as the system thermalizes in the disordered PM state. Finally, in the OP case, AFM correlations keep growing exponentially and the final thermal state is expected to be ordered. The detailed long-time evolution in this state depends on inhomogeneities present in any real system and requires a fully self-consistent treatment of the emerging order parameter, which is beyond the scope of this paper.

Figure 2 shows examples of the evolution of the instantaneous momentum distribution $n_{\boldsymbol{k}}(t) = \frac{1}{2} - \frac{i}{2} G^{\mathrm{K}}_{\boldsymbol{k}}(t,t)$ and spin-spin correlation function $i\chi^{\mathrm{K}}_{\boldsymbol{q}_0}(t,t)$ for $T_{\mathrm{i}} = 0$ and $U_{\mathrm{f}} = 3$ in the TSO regime ($t_{\mathrm{r}} = 0.5, 1$) and the OP regime ($t_{\mathrm{r}} = 2$). As discussed before, γ_{th} and T_{f} decrease with increasing t_{r}, such that prethermal regimes are maintained for longer times. This allows the AFM correlations in the TSO regime to grow to sizable values, as seen in Fig. 2(d). Since $T_{\mathrm{f}} > T_c^{\mathrm{eq}}$, $i\chi^{\mathrm{K}}_{\boldsymbol{q}_0}(t,t)$ is eventually expected to subside to the thermal equilibrium result in those cases. The regime OP is realized in Fig. 2(c) where the ramp time $t_{\mathrm{r}} = 2$ is longer, the heating is lower, and the system can thermalize in the ordered phase.

Finally, the growth of AFM correlations in real space after the ramp can be seen by calculating $\chi^{\mathrm{K}}(t,\boldsymbol{r}) = \frac{1}{N}\sum_{\boldsymbol{q}} e^{i\boldsymbol{q}\boldsymbol{r}}\, \chi^{\mathrm{K}}_{\boldsymbol{q}}(t,t)$, as shown in Fig. 3 for $t_{\mathrm{r}} = 1$ (TSO), 2 (OP). A clear AFM pattern develops once $i\chi^{\mathrm{K}}_{\boldsymbol{q}_0}(t,t)$ has grown to large enough values.

IV. CONCLUSIONS

We have studied the evolution and interplay of fermionic quasiparticles and collective magnetic correlations in the Hubbard model at half-filling following an interaction ramp, and have identified three regimes of qualitatively different dynamical behavior. Of particular interest is the occurrence of a parameter regime in which the prethermal state is marked with strong but transient AFM correlations.

The nonequilibrium phenomena discussed here can be probed in ultracold atoms experiments using measurements of local spin correlations [64,65], Bragg scattering of light [66], time-of-flight, and noise correlation measurements [67–69] once low enough temperatures are achieved. In fact, a significant enhancement of the AFM correlations has been reported recently [66,70]. We point out that questions addressed in this paper are generally important for the many ongoing experimental efforts for realizing quantum simulators of the fermionic Hubbard model. Inelastic losses in the vicinity of Feshbach resonances are fast and the experiments need to be performed rapidly to avoid strong heating of the atoms. Separating transient dynamical phenomena from equilibrium properties is crucial for drawing conclusions from such experiments.

Our work further opens the interesting new direction of designing protocols to realize novel many-body states using metastable prethermal states, in particular, states which may not be realized in equilibrium. Finally, our results show that fermionic systems with gapless excitations can introduce new features to the Kibble-Zurek picture of domain formation and coarsening in the dynamical crossing of phase boundaries discussed in the context of purely bosonic systems [71–73].

ACKNOWLEDGMENTS

We wish to thank E. dalla Torre, J. Freericks, S. Kehrein, M. Kollar, M. Knap, A. Millis, J. Han, A. Polkovnikov, M. Schiro, and P. Strack for insightful discussions. J.B. acknowledges financial support from the Deutsche Forschungsgemeinschaft through Grant No. BA 4371/1-1. M.B. was supported by the Institute for Quantum Information and Matter, an NSF Physics Frontiers Center with support of the Gordon and Betty Moore Foundation. We also acknowledge support from NSF Grant No. DMR-1308435, Harvard-MIT CUA, DARPA OLE program, AFOSR Quantum Simulation MURI, AFOSR MURI on Ultracold Molecules, the ARO-MURI on Atomtronics, and ARO MURI Quism program.

[1] R. Matsunaga, Y. I. Hamada, K. Makise, Y. Uzawa, H. Terai, Z. Wang, and R. Shimano, Phys. Rev. Lett. **111**, 057002 (2013).

[2] R. Matsunaga, N. Tsuji, H. Fujita, A. Sugioka, K. Makise, Y. Uzawa, H. Terai, Z. Wang, H. Aoki, and R. Shimano, Science **345**, 1145 (2014).

[3] L. Perfetti, P. A. Loukakos, M. Lisowski, U. Bovensiepen, H. Eisaki, and M. Wolf, Phys. Rev. Lett. **99**, 197001 (2007).

[4] S. Dal Conte, C. Giannetti, G. Coslovich, F. Cilento, D. Bossini, T. Abebaw, F. Banfi, G. Ferrini, H. Eisaki, M. Greven *et al.*, Science **335**, 1600 (2012).

[5] B. Mansart, M. J. Cottet, T. J. Penfold, S. B. Dugdale, R. Tediosi, M. Chergui, and F. Carbone, Proc. Natl. Acad. Sci. **109**, 5603 (2012).

[6] C. L. Smallwood, J. P. Hinton, C. Jozwiak, W. Zhang, J. D. Koralek, H. Eisaki, D.-H. Lee, J. Orenstein, and A. Lanzara, Science **336**, 1137 (2012).

[7] D. Fausti, R. Tobey, N. Dean, S. Kaiser, A. Dienst, M. Hoffmann, S. Pyon, T. Takayama, H. Takagi, and A. Cavalleri, Science **331**, 189 (2011).

[8] W. Hu, S. Kaiser, D. Nicoletti, C. R. Hunt, I. Gierz, M. C. Hoffmann, M. Le Tacon, T. Loew, B. Keimer, and A. Cavalleri Nat. Mater. **13**, 705 (2014).

[9] R. I. Tobey, D. Prabhakaran, A. T. Boothroyd, and A. Cavalleri, Phys. Rev. Lett. **101**, 197404 (2008).

[10] F. Schmitt, P. S. Kirchmann, U. Bovensiepen, R. G. Moore, L. Rettig, M. Krenz, J.-H. Chu, N. Ru, L. Perfetti, D. H. Lu *et al.*, Science **321**, 1649 (2008).

[11] W. Shen, Y. Ge, A. Y. Liu, H. R. Krishnamurthy, T. P. Devereaux, and J. K. Freericks, Phys. Rev. Lett. **112**, 176404 (2014).

[12] K. W. Kim, A. Pashkin, H. Schaefer, M. Beyer, M. Porer, T. Wolf, C. Bernhard, J. Demsar, R. Huber, and A. Leitenstorfer, Nat. Mater. **11**, 497 (2012).

[13] T. Kubacka, J. Johnson, M. Hoffmann, C. Vicario, S. De Jong, P. Beaud, S. Grübel, S.-W. Huang, L. Huber, L. Patthey *et al.*, Science **343**, 1333 (2014).

[14] M. Greiner, O. Mandel, T. W. Hänsch, and I. Bloch, Nature (London) **419**, 51 (2002).

[15] L. E. Sadler, J. M. Higbie, S. R. Leslie, M. Vengalattore, and D. M. Stamper-Kurn, Nature (London) **443**, 312 (2006).

[16] R. W. Cherng, V. Gritsev, D. M. Stamper-Kurn, and E. Demler, Phys. Rev. Lett. **100**, 180404 (2008).

[17] I. Bloch, J. Dalibard, and W. Zwerger, Rev. Mod. Phys. **80**, 885 (2008).

[18] G.-B. Jo, Y.-R. Lee, J.-H. Choi, C. A. Christensen, T. H. Kim, J. H. Thywissen, D. E. Pritchard, and W. Ketterle, Science **325**, 1521 (2009).

[19] A. Polkovnikov, K. Sengupta, A. Silva, and M. Vengalattore, Rev. Mod. Phys. **83**, 863 (2011).

[20] M. Cheneau, P. Barmettler, D. Poletti, M. Endres, P. Schauß, T. Fukuhara, C. Gross, I. Bloch, C. Kollath, and S. Kuhr, Nature (London) **481**, 484 (2012).

[21] C. Sanner, E. J. Su, W. Huang, A. Keshet, J. Gillen, and W. Ketterle, Phys. Rev. Lett. **108**, 240404 (2012).

[22] M. Ojekhile, R. Höppner, H. Moritz, and L. Mathey, arXiv:1308.5680.

[23] S. Braun, M. Friesdorf, S. S. Hodgman, M. Schreiber, J. P. Ronzheimer, A. Riera, M. del Rey, I. Bloch, J. Eisert, and U. Schneider, Proc. Natl. Acad. Sci. **112**, 3641 (2015).

[24] S. Trotzky, S. Beattie, C. Luciuk, S. Smale, A. B. Bardon, T. Enss, E. Taylor, S. Zhang, and J. H. Thywissen, Phys. Rev. Lett. **114**, 015301 (2015).

[25] D. Pekker, M. Babadi, R. Sensarma, N. Zinner, L. Pollet, M. W. Zwierlein, and E. Demler, Phys. Rev. Lett. **106**, 050402 (2011).

[26] J. Berges, S. Borsányi, and C. Wetterich, Phys. Rev. Lett. **93**, 142002 (2004).

[27] M. Moeckel and S. Kehrein, Phys. Rev. Lett. **100**, 175702 (2008).

[28] M. A. Cazalilla, Phys. Rev. Lett. **97**, 156403 (2006).

[29] S. R. Manmana, S. Wessel, R. M. Noack, and A. Muramatsu, Phys. Rev. Lett. **98**, 210405 (2007).

[30] C. Kollath, A. M. Läuchli, and E. Altman, Phys. Rev. Lett. **98**, 180601 (2007).

[31] M. Rigol, V. Dunjko, V. Yurovsky, and M. Olshanii, Phys. Rev. Lett. **98**, 050405 (2007).

[32] M. Rigol, V. Dunjko, and M. Olshanii, Nature (London) **452**, 854 (2008).

[33] M. Rigol, Phys. Rev. Lett. **103**, 100403 (2009).

[34] B. Dóra, M. Haque, and G. Zaránd, Phys. Rev. Lett. **106**, 156406 (2011).

[35] J. K. Freericks, V. M. Turkowski, and V. Zlatić, Phys. Rev. Lett. **97**, 266408 (2006).

[36] H. Aoki, N. Tsuji, M. Eckstein, M. Kollar, T. Oka, and P. Werner, Rev. Mod. Phys. **86**, 779 (2014).

[37] M. Eckstein, M. Kollar, and P. Werner, Phys. Rev. Lett. **103**, 056403 (2009).

[38] M. Moeckel and S. Kehrein, New J. Phys. **12**, 055016 (2010).

[39] M. Schiró and M. Fabrizio, Phys. Rev. Lett. **105**, 076401 (2010).

[40] M. Stark and M. Kollar, arXiv:1308.1610.

[41] A. Maraga, A. Silva, and M. Fabrizio, Phys. Rev. B **90**, 155131 (2014).

[42] R. A. Barankov, L. S. Levitov, and B. Z. Spivak, Phys. Rev. Lett. **93**, 160401 (2004).

[43] R. A. Barankov and L. S. Levitov, Phys. Rev. Lett. **96**, 230403 (2006).

[44] E. A. Yuzbashyan, O. Tsyplyatyev, and B. L. Altshuler, Phys. Rev. Lett. **96**, 097005 (2006).

[45] P. Werner, N. Tsuji, and M. Eckstein, Phys. Rev. B **86**, 205101 (2012).

[46] N. Tsuji, M. Eckstein, and P. Werner, Phys. Rev. Lett. **110**, 136404 (2013).

[47] M. Sandri and M. Fabrizio, Phys. Rev. B **88**, 165113 (2013).

[48] N. Tsuji and P. Werner, Phys. Rev. B **88**, 165115 (2013).

[49] In order that a true long range ordered state consistent with the Mermin-Wagner theorem is stable in the long-time limit, a small hopping in the perpendicular direction is assumed.

[50] P. G. J. van Dongen, Phys. Rev. Lett. **67**, 757 (1991).

[51] L. P. Gorkov and T. K. Melik-Barkhudarov, Sov. Phys. JETP **13**, 1018 (1961).

[52] A. Martin-Rodero and F. Flores, Phys. Rev. B **45**, 13008 (1992).

[53] H. Heiselberg, C. J. Pethick, H. Smith, and L. Viverit, Phys. Rev. Lett. **85**, 2418 (2000).

[54] A. Toschi, P. Barone, M. Capone, and C. Castellani, New J. Phys. **7**, 7 (2005).

[55] See Supplemental Material at http://link.aps.org/supplemental/10.1103/PhysRevB.92.024305 for additional details on the calculations described in the main text.

[56] G. Baym and L. P. Kadanoff, Phys. Rev. **124**, 287 (1961).

[57] L. V. Keldysh, Sov. Phys. JETP **20**, 1018 (1965).

[58] J. Rammer, *Quantum Field Theory of Non-equilibrium States* (Cambridge University Press, Cambridge, 2007).

[59] A. Kamenev, *Field Theory of Non-equilibrium Systems* (Cambridge University Press, Cambridge, 2011), Vol. 57.

[60] J. K. Freericks and D. J. Scalapino, Phys. Rev. B **49**, 6368 (1994).

[61] V. Zlatić, K. D. Schotte, and G. Schliecker, Phys. Rev. B **52**, 3639 (1995).

[62] A. Neumayr and W. Metzner, Phys. Rev. B **67**, 035112 (2003).

[63] Numerical inaccuracies can lead to discrepancies between the result of the long-time nonequilibrium calculation and the expected final state equilibrium result.
[64] J. Meineke, J.-P. Brantut, D. Stadler, T. Müller, H. Moritz, and T. Esslinger, Nat. Phys. **8**, 454 (2012).
[65] D. Greif, T. Uehlinger, G. Jotzu, L. Tarruell, and T. Esslinger, Science **340**, 1307 (2013).
[66] R. A. Hart, P. M. Duarte, T.-L. Yang, X. Liu, T. Paiva, E. Khatami, R. T. Scalettar, N. Trivedi, D. A. Huse, and R. G. Hulet, Nature (London) **519**, 211 (2015).
[67] S. Fölling, F. Gerbier, A. Widera, O. Mandel, T. Gericke, and I. Bloch, Nature (London) **434**, 481 (2005).
[68] M. Greiner, C. A. Regal, J. T. Stewart, and D. S. Jin, Phys. Rev. Lett. **94**, 110401 (2005).
[69] T. Rom, T. Best, D. Van Oosten, U. Schneider, S. Fölling, B. Paredes, and I. Bloch, Nature (London) **444**, 733 (2006).
[70] J. Imriška, M. Iazzi, L. Wang, E. Gull, D. Greif, T. Uehlinger, G. Jotzu, L. Tarruell, T. Esslinger, and M. Troyer, Phys. Rev. Lett. **112**, 115301 (2014).
[71] W. H. Zurek, U. Dorner, and P. Zoller, Phys. Rev. Lett. **95**, 105701 (2005).
[72] A. Polkovnikov, Phys. Rev. B **72**, 161201 (2005).
[73] R. W. Cherng and L. S. Levitov, Phys. Rev. A **73**, 043614 (2006).